Journal Pre-proof

Simultaneous, multiplex quantification of protease activities using a gold microelectrode array

Morgan J. Anderson, Yang Song, Huafang Fan, Jestin Gage Wright, Zhaoyang Ren, Duy H. Hua, Jessica E. Koehne, M. Meyyappan, Jun Li

PII: \$0956-5663(20)30325-0

DOI: https://doi.org/10.1016/j.bios.2020.112330

Reference: BIOS 112330

To appear in: Biosensors and Bioelectronics

Received Date: 4 May 2020 Revised Date: 22 May 2020 Accepted Date: 24 May 2020

Please cite this article as: Anderson, M.J., Song, Y., Fan, H., Wright, J.G., Ren, Z., Hua, D.H., Koehne, J.E., Meyyappan, M., Li, J., Simultaneous, multiplex quantification of protease activities using a gold microelectrode array, *Biosensors and Bioelectronics* (2020), doi: https://doi.org/10.1016/j.bios.2020.112330.

This is a PDF file of an article that has undergone enhancements after acceptance, such as the addition of a cover page and metadata, and formatting for readability, but it is not yet the definitive version of record. This version will undergo additional copyediting, typesetting and review before it is published in its final form, but we are providing this version to give early visibility of the article. Please note that, during the production process, errors may be discovered which could affect the content, and all legal disclaimers that apply to the journal pertain.

© 2020 Published by Elsevier B.V.



Morgan J. Anderson: Conceptualization, Methodology, Software, Validation, Formal analysis, Investigation, Writing - Original Draft, Visualization, Funding acquisition Yang Song: Conceptualization, Methodology, Validation, Investigation, Writing - Review & Editing, Visualization, Supervision Huafang Fan: Methodology, Investigation, Supervision, Visualization, Validation Jestin Gage Wright: Investigation, Validation Zhaoyang Ren: Investigation, Validation Duy H. Hua: Conceptualization, Methodology, Resources, Writing - Review & Editing, Project administration, Funding acquisition, Formal analysis, Supervision, Project administration M. Meyyappan: Resources, Writing - Review & Editing, Funding acquisition, Formal analysis Jun Li: Conceptualization, Methodology, Resources, Writing - Review & Editing, Supervision, Project administration, Formal analysis

Journal Pre-proof

Simultaneous, Multiplex Quantification of Protease Activities Using a Gold Microelectrode Array

Morgan J. Anderson^{a,b,*}, Yang Song^a*, Huafang Fan^a, Jestin Gage Wright^a, Zhaoyang Ren^a, Duy H. Hua^a, Jessica E. Koehne^c, M. Meyyappan^c, and Jun Li^{a,**}

^a Department of Chemistry, Kansas State University, Manhattan, KS 66506-0401, United States

^b Universities Space Research Association, NASA Ames Research Center, Moffett Field, CA 94035, United States

^c NASA Ames Research Center, Moffett Field, CA 94035, United States

^{*} These authors contributed equally to this work.

^{**} Corresponding Author: Phone: +1 785 532 0955; fax: +1 785 532 6666; E-mail: junli@ksu.edu (J. Li)

Abstract

Proteases are a large family of enzymes involved in many important biological processes.

Quantitative detection of the activity profile of specific target proteases is in high demand for the

diagnosis and monitoring of diseases such as cancers. This study demonstrates the fabrication

and characterization of an individually addressable 3x3 Au microelectrode array for rapid,

multiplex detection of cathepsin B activity based on a simple electrochemical method. The nine

individual microelectrodes in the array show highly consistent cyclic voltammetric signals in Au

surface cleaning experiments and detecting benchmark redox species in solution. The individual

Au microelectrodes are further selectively functionalized with specific ferrocene-labeled peptide

molecules which serve as the cognate substrates for the target proteases. Consistent proteolytic

kinetics are measured by monitoring the decay of the AC voltammetry signal from the ferrocene

label as the peptide molecules are cleaved by cathepsin B. Accurate activity of cathepsin B is

derived with an improved fitting algorithm. Simultaneous detection of the proteolysis of

cathepsin B on the microelectrode array functionalized with three different hexapeptides is

demonstrated, showing the potential of this sensor platform for rapid detection of the activity

profiles of multiple proteases in various diseases including many forms of cancer.

Keywords: Protease activity, Microelectrode array, AC Voltammetry, Cathepsin B, Proteolysis

2

1. Introduction

Proteases are a class of enzymes, which selectively break down proteins by targeting the specific constituent peptide sequences and cleaving the peptide bonds at specific sites. (López-Otín and Overall, 2002; Turk, 2006; Turk et al., 2012) About 600 different proteases have been identified in humans, which have an active role in many cellular processes including apoptosis, angiogenesis, hormone activation, etc.(Turk et al., 2012) Their overexpression has been found to be indicative of several diseases and medical conditions such as muscle atrophy (Morris et al., 2005; Nagaraj and Santhanam, 2006) and cancer progression (Koblinski et al., 2000; López-Otín and Matrisian, 2007; Rakashanda et al., 2012). Because of their prevalence and selectivity, proteases can serve as biomarkers for medical diagnostics and targets for therapeutic drugs such as protease inhibitors. (Lee et al., 2004; Turk, 2006) Developing rapid low-cost techniques that can quantitatively detect multiple proteases is essential for these applications.

Several methods exist currently for rapid protease quantification and the diagnostic assays fall into two categories. The first type focuses on the quantification of the overall concentration of the protease, for example, the widely used commercial enzyme-linked immunosorbent assays (ELISA) such as the Quantikine® Human Pro-Cathepsin B ELISA kit by R&D Systems Inc., and various immunohistochemical assays (Jacquemier et al., 2005; Leelawat et al., 2009). These affinity-based methods use specific antibodies to selectively bind the target proteases, but they normally cannot distinguish the inactive proenzymes from the active enzymes, thus cannot provide accurate information regarding the biological functions of the proteases.

The second category focuses on quantification of the activity of specific protease enzymes, i.e. the overall rate of the proteolysis reactions that are induced by the specific amount

of particular proteases. Fluorogenic assays that measure the increase in fluorescence emission upon cleavage of a quenched fluorophore in a peptide substrate by the cognate protease are representative examples of such activity-based techniques. (Ong and Yang, 2017; Sanman and Bogyo, 2014) These activity-based approaches are advantageous because they account for the fact that not all the protease enzymes are active and that the effectiveness of the proteases can vary drastically from different sources. More importantly, the enzyme activity not only depends on the concentration of the active enzyme but also the measuring conditions such as the cognate peptide substrate, buffer composition, temperature and presence of inhibitors. By measuring the kinetic profile of the fluorogenic signal from the cleaved peptide products, the proteolytic reaction rate can be derived, which directly reflects the biochemically relevant activities of the proteases.

Electrochemical methods for quantification of protease activity have shown great promise recently. (Liu et al., 2006; Ohtsuka et al., 2009; Puiu and Bala, 2017; Song et al., 2019; Swisher et al., 2015; Swisher et al., 2014; Swisher et al., 2013; Wang et al., 2020) The measurements typically rely on a peptide substrate having a terminal redox moiety, often ferrocene (Fc), immobilized onto an electrode surface. The concentration of the electrode-bound redox probe provides a baseline signal, which can be observed by common electrochemical techniques such as cyclic voltammetry (CV), square wave voltammetry (SWV), differential pulse voltammetry (DPV) and AC voltammetry (ACV). The decrease in the electrochemical signal reflects the rate of peptide substrate proteolysis by the cognate protease. In our previous studies, (Song et al., 2019; Swisher et al., 2015; Swisher et al., 2014; Swisher et al., 2013) we have found (based on a heterogeneous Michaelis-Menten enzymatic model) that the electrochemical signal decays exponentially with regard to the reaction time and the inverse of the decay time constant, i.e. $1/\tau$,

directly reflects the protease activity. This method has been successfully demonstrated for the measuring the activity of cathepsin B, a cancer-related protease, in simple buffer solutions (Song et al., 2019; Swisher et al., 2013) as well as complex samples including tissue lysates (Swisher et al., 2014) and cell lysates (Swisher et al., 2015) using a nanoelectrode array fabricated with vertically aligned carbon nanofibers.

Furthermore, electrochemical methods can be adapted to individually addressed microelectrode arrays (MEAs) for highly multiplex detection. (Arumugam et al., 2009; Koehne et al., 2004; Radke and Alocilja, 2005) Selectively functionalizing individual electrodes with peptide substrates that are specific to their cognate proteases allows mitigation of complicated cross-reactions and cascade networks of related proteases; this is enabled by collectively analyzing the activity profiles derived from the sensor arrays, similar to the mechanism that allows an array of sensory receptors in the tongue to distinguish complicated flavors. (Podražka et al., 2018) In this study, we have extended our previously demonstrated electrochemical method into a 3 x 3 Au MEA and demonstrate its capability for the simultaneous detection of cathepsin B activities using three different peptide substrates functionalized on the MEA. The fitting algorithm has also been refined to obtain more accurate results. The results from the nine electrodes in the MEA are highly consistent, enabling its applications for reliable screening of peptide substrate candidates. These advances lay the foundation for future multiplex electronic chips that can be used for rapid detection of protease activity profiles in disease diagnosis and treatment monitoring.

2. Materials and Methods:

2.1 Reagents:

N-Fluorenylmethyloxycarbonyl (Fmoc) protected amino acids, amino acid attached 2chlorotrityl resins, 1-[bis(dimethylamino)methylene]-1*H*-1,2,3-triazolo[4,5-b]pyridinium 3-oxide hexafluorophosphate (HATU), 2-(1*H*-benzotriazol-1-yl)-1,1,3,3-tetramethyluronium and hexafluorophosphate (HBTU) were purchased from Chem-Impex International, Inc. (Wood Dale, IL) and AAPPTEC LLC (Louisville, KY). Potassium hexacyanoferrate (II) trihydrate, potassium nitrate, 1-ethyl-3-(3-dimethylaminopropyl)carbodiimide (EDC), Nhydroxysulfosuccinimide (Sulfo-NHS), 6-mercapto-1-hexanol, and 6-mercapto-1-hexanoic acid were obtained from Sigma-Aldrich (St. Louis, MO). Dithiothreitol (DTT), sodium phosphate dibasic heptahydrate (Na₂HPO₄•7H₂O), sodium phosphate monobasic (NaH₂PO₄) and 2-(4morpholino)ethanesulfonic acid (MES) were purchased from Fisher Scientific (Hampton, NH). Purified recombinant human cathepsin B (~60% 37 kDa inactive form and ~40% 25 kDa active form) was acquired from R&D Systems Inc. (Minneapolis, MN). Cathepsin B solutions were activated by incubation in 25 mM MES buffer (pH = 5.0) containing 5 mM DTT for 15 min before proteolysis experiments.

2.2 Electrochemical Measurements:

Electrochemical measurements were performed using an Ivium n-Stat Potentiostat (Eindhoven, The Netherlands) outfitted with five dual channel modules, allowing up to ten independent working electrodes to function simultaneously with a common reference and counter electrodes. The experimental setup is shown in Figure S1 in the Supporting Information (SI). Figure S1a shows a block diagram of the experimental setup. In this study, the nine leads from the potentiostat (Figure S1b) were interfaced with a breakout box, which was then connected to a custom-built electrochemical cell via a ribbon cable (Figure S1c). The sensor chip

consists of nine lithographically patterned Au working microelectrodes placed in the custom-built electrochemical cell (Figure S1d) and electrical contact was made via pogo pins. All measurements were performed using a common mercury/mercurous sulfate reference electrode (Hg/Hg₂SO₄, MSE) filled with a saturated solution of K₂SO₄ (CH Instruments, Austin, TX) and a common Pt wire counter electrode.

2.3 Device Fabrication:

Device fabrication was performed at the Stanford Nanofabrication Facility (Stanford, CA). A workflow of the wafer-scale fabrication process is shown in Scheme S1 in the SI. Thermal oxidation of standard 4" Si<100> wafers was performed by ramping the temperature to 1100 °C and holding for 45 min in the presence of gaseous H₂O. This produced a thermal oxide with a thickness of ~550 nm. Next, the wafers were coated with 20 nm Ti, 100 nm Au and another 20 nm Ti by electron beam evaporation (Innotec ES26C, Battle Ground, WA). The wafers were then spin-coated with an automated spin-coating track (SVG 8400, San Jose, CA) with 1.0 µm SPR3612 positive photoresist (Rohm and Haas Electronic Materials, Marlborough, MA) and exposed on a mask aligner (Karl Suss MA-1, Garching, Germany) with an exposure dose of 80 mJ/cm² (exposure time = 5.3 s) through a chrome photomask (FrontRange Photomask, Lake Havasu City, AZ). Next, the wafers were developed with an automated developing track (SVG 8600, San Jose, CA), leaving the electrode MEA design patterned in photoresist. The exposed areas on the wafers were then etched with a ratio of 1:50 of HF:H₂O to remove the top layer of Ti, with Transene TFA Au etchant to remove the Au layer, and again with 1:50 HF:H₂O to remove the bottom layer of Ti, leaving the MEA pattern (including contact pads, leads and the microelectrode surface). After etching, the photoresist was stripped off and a 1-μm thick layer of SiO₂ was deposited over the entire wafer by plasma-enhanced chemical

vapor deposition (PE-CVD, Plasma-Therm Shuttlelock SLR-730-PECVD, St. Petersburg, FL) with 250 sccm 5% SiH₄/He, 800 sccm He and 1700 sccm N₂O at 350 °C, 1100 mTorr and 200 W for 15 min. Next, the SiO₂-coated substrate was spin-coated with a 1.0-μm layer of SPR3612 positive photoresist and subsequently exposed with an exposure dose of 80 mJ/cm² leaving the SiO₂ over the microelectrode surface and the contact pads exposed. The exposed SiO₂ was etched with CHF₃ plasma (2 sccm O₂ and 45 sccm CHF₃ at 5.0 mTorr for 8 min) using a reactive ion etcher (RIE, Plasma-Therm Versaline LL-ICP, St. Petersberg, FL), and then the top layer of Ti was etched with HF and H₂O (1:50) to expose the Au surface. Finally, the wafers were coated with a 5.0-μm layer of SPR3612 as a protective layer and the individual chips were diced with a wafer saw (DISCO DAD3240, Tokyo, Japan). Prior to use, the chips were sonicated in acetone and sequentially rinsed with acetone, methanol and isopropanol to remove any residual photoresist. Figure S2 illustrates the top and side view of the MEA structure and Figure S3 shows the SEM characterization of the fabricated Au MEAs.

2.4 Peptide Synthesis:

A library of nine peptide substrates was examined initially for proteolysis using cathepsin B (Table S1) As described previously, tetra-, hexa- and octa-peptide substrates having similar sequences have been used, and hexapeptides were found to yield the optimal signal (Song et al., 2019). The order and amino acid sequence of the peptide substrates were designed according to the literature reported sequences with minor modifications. Among the nine peptides, three most reactive peptide substrates, i.e. H-3, H-15, and H-16 (Table 1), were selected for our studies on cathepsin B activity profiling. The peptides were synthesized using a solid-phase microwave peptide synthesizer detailed in the SI. For example, peptide H-15, a representative peptide, was made by the coupling of H-Ala-2-chlorotrityl resin with various *N*-fluorenylmethyloxycarbonyl-

amino acids (*N*-Fmoc-amino acids) sequentially, condensing with the linker *N*-Boc-NH-(CH₂)₄-CO₂H, cleavage of the peptide from the resin, re-protection of the amino group of linker, bonding with (aminomethyl)ferrocene, and removal of the protecting group.

Table 1: Hexapeptide Sequences

Peptide Name	<u>Structure</u>
H-3	H ₂ N-(CH ₂) ₄ -CO-Pro-Leu-Arg-Phe-Gly-Ala-NH-CH ₂ -Fc
H-15	H ₂ N-(CH ₂) ₄ -CO-Pro-Leu-Ala-Phe-Val-Ala-NH-CH ₂ -Fc
H-16	H ₂ N-(CH ₂) ₄ -CO-Pro-Leu-Ala-Gly-Val-Ala-NH-CH ₂ -Fc

2.5 Electrode Preparation:

Prior to use, the MEAs were sonicated in acetone for 1 minute, subsequently rinsed with methanol and isopropanol for 15 s and then dried by blowing with nitrogen. Next, the electrodes were placed in the experimental cell and electrochemically cleaned by cycling from -0.60 to 0.70 V vs. MSE in 0.10 M phosphate buffer (pH = 7.4). For the experiments using an MEA modified with the same peptide-Fc substrate (i.e. H-15) on all nine microelectrodes, the whole chip was incubated in a mixture of 1.0 mM 6-mercapto-1-hexanol and 0.2 mM 6-mercapto-1-hexanoic acid in deionized water for 40 min to form a self-assembled monolayer (SAM). This step passivated the entire Au microelectrode surface while leaving adequate spacing between the exposed carboxyl functionalities. Next, the electrodes were incubated in a solution containing 2.0 mM peptide-Fc substrate (i.e. H-3, H-15, or H-16), 0.20 g/l EDC and 0.20 g/l sulfo-NHS for 2 hours at room temperature so that the peptides were covalently attached to the carboxyl groups of the SAM through the formation of amide bonds. The low ratio of carboxyl to hydroxyl groups at the SAM surface ensured a large separation between the peptide-Fc molecules which was important to reduce the steric hindrance during subsequent proteolysis measurements. Finally,

the electrodes were rinsed with deionized water to remove any non-bound peptide-Fc substrate that may be physiosorbed on the surface. For multiplex experiments, the chip was masked with a ~1.2 mm thick polydimethylsiloxane (PDMS) film punched with a 3x3 array of ~0.7 mm diameter holes that were aligned on top of each Au microelectrodes. About 100 μl mixed thiol solution (6-mercapto-1-hexanol and 6-mercapto-1-hexanoic acid) as described above was added on the chip surface to fill all nine PDMS holes and was incubated for 40 min. Then, the microelectrodes and wells were rinsed and dried on a hot plate at 35 °C. Finally, 0.50 μl of the EDC/sulfo-NHS/peptide-Fc (H-3, H-15, or H-16) reaction mixture was added to each well using a nanoinjector mounted on a x-y-z- micromanipulator and incubated for 2 h. The functionalized MEA was then rinsed with DI water and immediately used for the proteolysis measurements.

2.6 Proteolysis Measurements:

Proteolysis experiments were performed around 37 °C using a heat sink plate fabricated from a copper block with a drilled through-hole and fittings to circulate heated silicone liquid from a thermal circulator (Julabo F12, Allentown, PA). The MEA chip was mounted on the copper block and the thermal circulator was set at 41.2 °C in order to maintain the MEA at about 38.6 °C. Cathepsin B solutions were activated by incubation in 25 mM MES buffer (pH = 5.0) containing 5.0 mM DTT for 15 min prior to proteolysis experiments. About 10 μ 1 activated cathepsin B was added into the electrochemical cell containing 815 μ 1 assay buffer, i.e. 25 mM MES buffer (pH = 5.0). Continuously repeated ACV (with an AC frequency of 300 Hz and 100 mV amplitude superimposed on a DC ramp from -0.45 V to 0.20 V vs. MSE) was recorded over the independently addressed 3x3 MEA for a period starting from about 5 - 10 min before adding the activated protease solution to about 85 min afterwards.

3. Results and Discussion:

3.1 Microelectrode Array Design:

Microfabricated chips are commonly used in multiplex electrochemical sensor devices. However, careful planning is needed to ensure that the microfabricated chips are suitable for the specific applications. In the current study, 3x3 Au microelectrode arrays (MEAs) were fabricated so that measurements could be performed simultaneously on nine independently operating electrodes. Figure 1a shows the schematic of the MEA chip design with a zoomed-in portion on the right side to indicate the numbering scheme of the MEA. The microelectrodes were $200 \, \mu m \, x \, 200 \, \mu m$ and separated by $1000 \, \mu m$ to provide enough space to individually functionalize each electrode. The contact pads (lined up in the row at the bottom) were $1000 \, \mu m \, x \, 1000 \, \mu m$ to provide adequate space for electrical contact via pogo pins outside the electrochemical cell. The on-chip leads from the contact pads to the electrodes were $20 \, \mu m$ wide, providing good electrical connections at low resistance ($\sim 110 \, \Omega$). Figure 1b shows an optical micrograph of the whole chip and Figure 1c shows a zoom-in optical image of the MEA similar to the numbering scheme in Figure 1a.

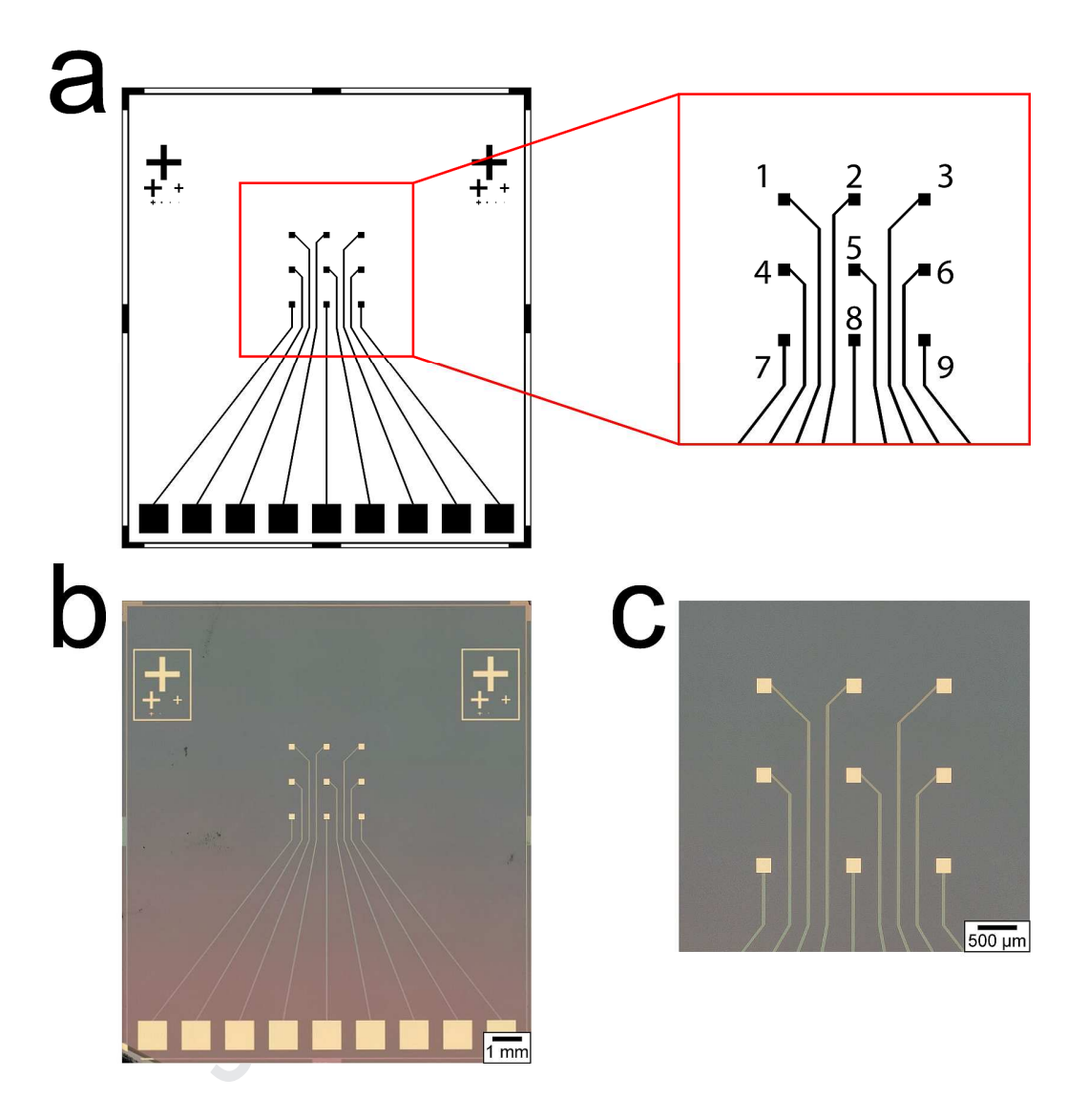


Figure 1: (a) Schematic diagram of the Au MEA chip layout with a zoom-in picture (right side) to illustrate the channel numbering scheme. (b) and (c) Optical micrographs of a fabricated Au MEA chip.

Figure S2 in the SI shows the top and side views illustrating the structure of the MEA chip. The fabrication protocol is described in detail in the Experimental Section and Scheme S1 in the SI, but the structure is discussed briefly here. The chips were fabricated on 100 mm Si wafers with a 550 nm layer of thermally grown SiO_2 as an insulating dielectric. Each wafer

contains 20 MEA chips. The electrodes, leads and contact pads consisted of a 20-nm Ti adhesion layer and 100 nm Au. Figure S3a is an SEM micrograph of the exposed Au showing the individual grains of the Au film. An additional 20-nm adhesion Ti layer was patterned onto the electrode leads and a 1.0-µm SiO₂ dielectric layer was deposited and patterned to insulate the leads and the chip surface while leaving the microelectrodes and contact pads exposed. As shown in Figure S3b, the top SiO₂ surface is significantly rougher than the exposed Au and significant charging is observed in the micrograph due to the insulating nature of the SiO₂ dielectric layer.

The exposed microelectrodes and contact pads appear in gold color in Figures 1b and 1c while the leads buried underneath SiO_2 appear in blue. Figure S3c shows an electron micrograph of the boundary between the topmost SiO_2 layer and the exposed Au of the electrode. It is clear that the 200 μ m x 200 μ m microelectrode is not fully exposed. A small portion (~ 3-7 μ m wide) of the Au microelectrode, particularly at the corner, is embedded underneath the SiO_2 dielectric layer. This only induces very small variations in the microelectrode area but is not expected to impact the proteolysis measurements in this study. In fact, it prevents the Ti underlayer from being exposed at the edge of the electrode and helps to make the Au MEAs more stable and useable repeatedly.

3.2 Cyclic Voltammetry Characterization:

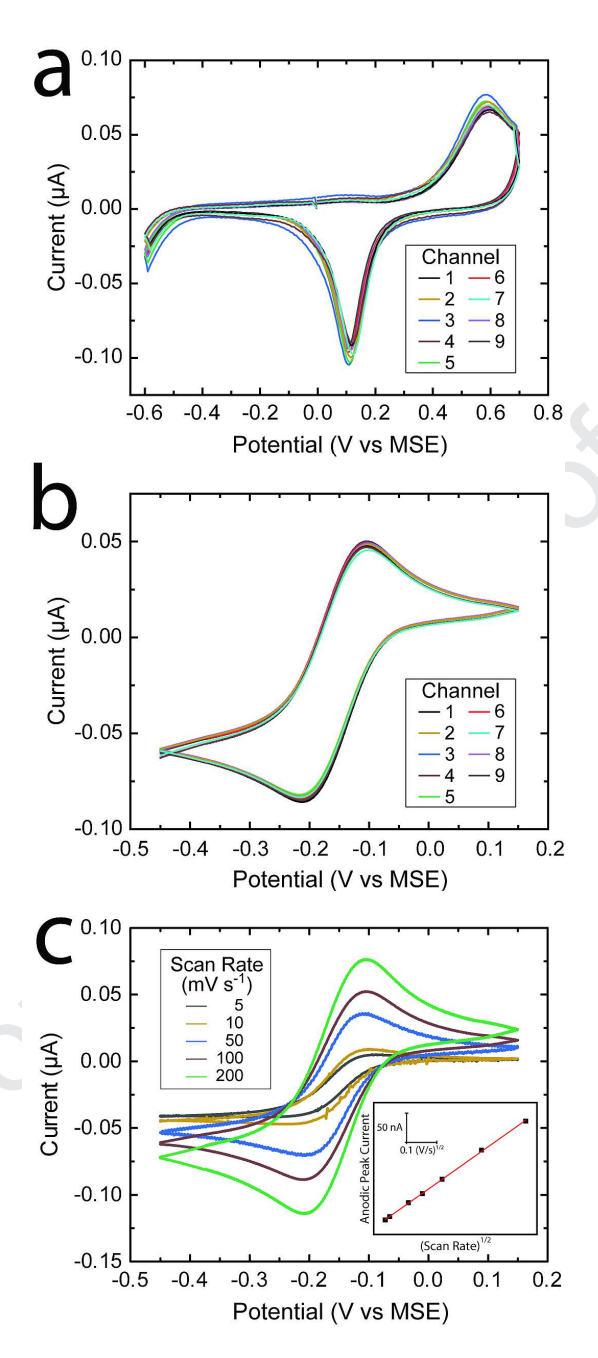


Figure 2: Electrochemical characterization of an insulated, unmodified MEA chip. (a) Electrochemical oxidation of Au performed in 0.10 M phosphate buffer (pH = 7.4). The measurements were performed on all nine channels simultaneously with scan rate (v) = 100 mV/s. (b) Simultaneous, multiplex measurement of Fe(CN)₆⁴⁻ oxidation on all nine channels simultaneously. The measurements were obtained in a solution containing 1.0 mM K₄Fe(CN)₆ and 0.10 M KNO₃ with a v = 100 mV/s. (c) The dependence of v on Fe(CN)₆⁴⁻ oxidation. The measurements were obtained using only channel 5 in a solution containing 1.0 mM K₄Fe(CN)₆ and 0.10 M KNO₃.

Electrochemical characterization is crucial to ensuring that the MEAs are suitable for sensing applications. Cyclic voltammetry (CV) is the most common method for characterizing the electrochemical behavior of sensors. CV measurements of well-known electrochemical processes can be used to evaluate the electrode surface and charge transfer kinetics.

Electrochemical cleaning of Au is a common characterization method for evaluating the quality of Au electrodes. These measurements were performed by sweeping the Au electrode potential from -0.60 to 0.70 V vs. MSE and back for 10 full cycles. Typically, Au cleaning on bulk electrodes is performed in 0.10 M H₂SO₄. However, cycling at low pH appears to cause dissolution and delamination of both Au surface and the underlying Ti adhesion layer. Consequently, these experiments were performed in phosphate buffer (pH = 7.4), which has been reported previously. (Anderson and Crooks, 2014; Oesch and Janata, 1983a, b) Figure 2a shows the tenth complete cycle of an electrochemical Au cleaning performed simultaneously on all nine electrodes. The potential begins at -0.60 V and a slightly negative current is observed due to the onset of hydrogen production by water electrolysis. As the applied potential is increased (moving from left to right), the current increases to $\sim 0 \mu A$ indicating that no electrochemical reaction takes place. As the potential continues to move in the positive direction, the current becomes more positive, resulting in a localized peak at 0.60 V. This anodic current is indicative of the formation of Au₂O₃ on the electrode surface. The potential sweep continues to 0.70 V, which is known to form a complete monolayer of Au₂O₃ on the electrode surface. (Anderson and Crooks, 2014; Oesch and Janata, 1983a, b; Rodríguez-López et al., 2008)

The potential sweep is then reversed. As the potential continues to move in the negative direction, a cathodic peak emerges at 0.11 V vs. MSE. This peak arises from the reduction of

 Au_2O_3 to Au, and the charge associated with the peak is directly related to the number of Au atoms present on the electrode surface. The average peak height is -94.3 \pm 4.7 nA across all nine electrodes, indicating that they all behave consistently with very similar exposed Au surface areas. These Au cleaning CVs show the characteristic features of clean polycrystalline Au electrodes.

Another common voltammetric characterization technique is the oxidation of a benchmark K_4 Fe(CN)₆ species as shown in Figure 2b. Here, the electrodes are cycled between -0.45 to 0.15 V vs. MSE at a scan rate (ν) of 100 mV/s in a solution containing 1.0 mM K_4 Fe(CN)₆ and 0.10 M KNO₃. Initially, the electrode potential is swept in the positive direction beginning at -0.45 V vs. MSE. As the potential increases, the anodic current increases due to the oxidation of Fe(CN)₆⁴⁺ to Fe(CN)₆³⁻ and forms a peak at -0.11 V vs. MSE followed by a gradual decay in the current. Upon reversing the potential sweep at 0.15 V vs. MSE, similar behavior is observed in the cathodic direction showing a peak at -0.21 V vs. MSE. The peak separation was 0.10 V, in agreement with similar studies of the Fe(CN)₆^{3-/4-} redox couple. (Hua et al., 2019) The observed half peak potential ($E_{1/2}$) was -0.16 V vs. MSE. The average anodic and cathodic peak heights for all nine channels were 79.0 \pm 1.8 nA and -80.9 \pm 1.3 nA, respectively, demonstrating good agreement across all nine microelectrodes. This behavior is typical for electrochemical reactions of solution-based redox species.

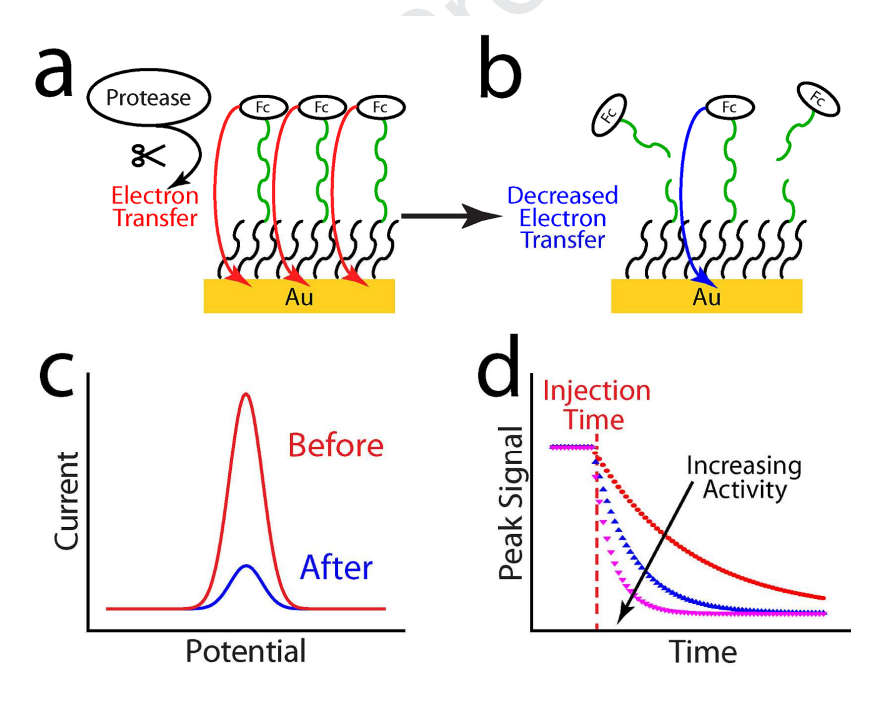
The final electrochemical characterization performed here with benchmark species was the examination of the dependence of v on the oxidation/reduction of Fe(CN)₆⁴⁻ by CV. Varying v allows for evaluation of the mass-transport properties of the electrochemical reaction. (Wightman, 1981) Changes in the shape of the current transient and i_p with v provide information about the electrode geometry and the electrochemical reaction. Figure 2c shows several CVs

obtained on the same microelectrode, channel (CH) 5, at different values of v. The CV trace shows a sigmoidal shape at the lowest value of v (5 mV/s, black line). This sigmoidal shape is a characteristic electrochemical behavior of microelectrodes and occurs because the radial diffusion at the electrode edges is relatively larger than the linear diffusion normal to the electrode surface, resulting in a mass-transport limited steady-state current. Slow values of v allow more time for the diffusion layer to grow and reach the steady state. As v increases to 10 mV/s (yellow line), small anodic and cathodic peaks emerge at -0.102 V and -0.233 V, respectively. At higher values of v, the reactants near the electrode surface are depleted faster than diffusion layer development. As v further increases to 50 mV/s (blue line), the anodic and cathodic peaks shift to -0.116 V and -0.206 V, respectively, and the peak heights increase. At even higher values of v, the peak potentials remain relatively constant and the peak heights continue to increase. The inset of Figure 2c shows a plot of the anodic values of i_p vs. $v^{1/2}$. The data for anodic i_p demonstrates a linear relationship with $v^{1/2}$, indicating that the observed signal is dominated by linear diffusion relative to radial diffusion. This is typical for electrochemical reactions of solution-based species under diffusion-controlled conditions. These results demonstrate that our Au MEAs behave as expected and are suitable for use as electrochemical sensors.

3.3 Multiplex Proteolysis:

After validation using optical and electrochemical characterizations, the MEAs were used to develop a sensor for the simultaneous, selective detection of protease activities. This was achieved by modifying the electrode surface with a SAM in an aqueous solution of mercaptohexanol and mercaptohexanoic acid and then tethering the peptide-Fc substrate to the exposed carboxyl groups, as described in the Experimental Section. CV characterization using

an Au disk electrode of 2.0 mm diameter (Figure S4) reveals the density of functionalized peptide-Fc (Γ) using this protocol to be about 30.3 pmol/cm², giving an average spacing of 2.46 nm. The actual spacing may be larger because the effective surface area is often larger than the geometric surface area. (Bard and Faulkner, 2001; Oesch and Janata, 1983a, b) Such surface concentration is significantly lower than the maximum expected surface coverage for a close-packed Fc-terminated SAM (460 pmol/cm²). (Collard and Fox, 1991) The low density allows adequate space between the peptide chains for proteolysis reactions to occur without significant steric hindrance while passivating the electrode surface to decrease capacitance, thus improving the signal-to-noise ratio in the electrochemical measurements.



<u>Figure 3.</u> Schematic illustration of the proteolysis sensing mechanism. (a) The electrode before and (b) after a proteolysis reaction. The gold box represents the Au electrode surface, the wavy black lines are the alkanethiols bound to the electrode surface and the green wavy lines are the exposed Fc-terminated peptide sequence. (c) The schematic ACV curves before and after proteolysis. (d) The schematic kinetic proteolysis curves at varied protease activities.

The sensing strategy is illustrated in Figure 3. The left side of Figure 3a shows a cartoon of the electrode prior to any proteolysis reaction. The gold box represents the Au electrode surface, the wavy black lines are the alkanethiols bound to the electrode surface and the green wavy lines are the exposed Fc-terminated peptide sequence. Here, all the Fc tags can be oxidized into ferrocenium (Fc⁺) by transferring electrons to the electrode as depicted by the red arrows. This electron transfer corresponds to an ACV peak depicted by the red trace in Figure 3b. An experimental example of the unprocessed ACV obtained from a peptide-Fc modified Au microelectrode is shown in Figure S5a in the SI. The black trace shows the experimental signal, which revealed a Gaussian peak near -0.05 V vs. MSE on top of a tilted background as shown by the red line in Figure S5a. The baseline is subtracted from the ACV curve to result in a well-defined peak as shown in Figure S5b.

When the target protease is added to the sample chip, it cleaves the peptides, causing the tethered Fc-moieties to diffuse away from the electrode surface. This leads to a decrease of electron transfer as illustrated by the blue arrow on the right half of Figure 3a. As a result, the ACV peak becomes smaller as represented by the blue trace in Figure 3b. Figure 3d shows a theoretical plot of the ACV peak height (i_p) vs. time of the proteolytic reaction where t = 0 min is defined as the first measurement after protease injection. These plots are hereafter referred to as proteolysis plots. Focusing first on the red curve, i_p is stable prior to the injection time. After the protease is injected into the electrochemical cell, the peak signal decays exponentially until approaching zero. As the activity of the protease increases, the proteolysis reaction rate is raised as depicted by the blue and pink curves, indicated by the faster decay in i_p .

Previously, (Song et al., 2019; Swisher et al., 2015; Swisher et al., 2014; Swisher et al., 2013) we have shown that this exponential decay in i_p corresponds to the proteolysis kinetics predicted by the Michaelis-Menten model for heterogeneous enzymatic reactions. (Gutiérrez et al., 2004) The model is based on the enzymatic reaction

$$E + S_S \stackrel{k_1}{\rightleftharpoons} ES_S \stackrel{k_{cat}}{\longrightarrow} E + P_S + P \tag{1}$$

where E is the enzyme, S_s is the intact surface-bound peptide-Fc substrate, ES_s is the enzyme-substrate complex, P_s is the surface bound peptide product remaining after the proteolytic cleavage, P is the Fc-tagged peptide fragment which is free to diffuse into solution, and k_l , k_{-l} and k_{cat} are the rate constants of the respective reactions. Based on this model, the decay in the experimental signal, v, is described as

$$\mathbf{v} = -\frac{d\Gamma_{SS}}{dt} = \frac{k_{cat}}{K_{M} + [E_{0}]} [E_{0}] \Gamma_{SS} , \qquad (2)$$

where Γ_{Ss} is the surface concentration of S_s and $K_M = (k_{cat} + k_{-I})/k_I$ is the Michaelis-Menten constant. Because $i_p \propto \Gamma_{Ss}$, we can write

$$\frac{\Gamma_{\rm S}}{\Gamma_{\rm S0}} = \frac{i_{\rm p}}{i_{\rm p0}} \ . \tag{3}$$

By making the assumption $K_M >> [E_0]$ and combining eq 2 and eq 3, we have:

$$-\frac{d^{i_p}/i_{p_0}}{dt} \approx \frac{k_{cat}}{K_M} [E_0] \binom{i_p}{i_{p_0}}, \qquad (4)$$

Integrating eq 4 with respect to i_p/i_{p0} yields:

$$t = \int -\frac{K_{M}}{k_{\text{cat}}[E_{0}]} \frac{1}{i_{p}/i_{p0}} d\binom{i_{p}}{i_{p0}} = -\frac{K_{M}}{k_{\text{cat}}[E_{0}]} ln\binom{i_{p}/i_{p0}}{i_{p0}},$$
 (5)

which can be rearranged to

$$i_p = i_{p0} exp \left[-\frac{t}{\tau} \right], \tag{6}$$

where $1/\tau$ is:

$$\frac{1}{\tau} = \left(\frac{k_{cat}}{K_{\mathsf{M}}}\right) [E_0] \tag{7}$$

The value of $1/\tau$ is defined as the activity of the target protease on the specific peptide-Fc substrate and directly corresponds to the decay rate of i_p .

While this model has been demonstrated in previous reports (Gutiérrez et al., 2004; Song et al., 2019; Swisher et al., 2014; Swisher et al., 2013), several non-idealities have been observed which we have sought to account for here. These non-idealities are highlighted in Figure S6 in the SI. First, as illustrated in Figure S6a, the baseline value of i_p decreased linearly prior to the injection of the target protease. This is attributed to the instability of the exposed Fc moiety. (González-Fernández et al., 2016; Kang et al., 2016) A linear term has been added to eq 6 to account for this:

$$i_p = a[exp(-t/\tau)] + bt + c$$
 (8)

and consequently, the value of i_{p0} is redefined as

$$i_{p0} = a + c (9)$$

Eq 8 has been used to fit the proteolysis data and derive the value of $1/\tau$ for each proteolysis measurement.

Furthermore, there is a large drop in signal after the cathepsin B is injected into the electrochemical cell. The cause of this large decrease is illustrated in Figures S6b and S6c which show ACV traces obtained at t = 0 min and t = 1.2 min, respectively. The data in Figure S6b can be fitted into two overlapping Gaussian peaks: the Fc signal peak at -0.101 V vs. MSE and an interference peak at -0.243 V vs. MSE. The cause of the interference peak is not clear yet, but it was observed to be present in ACV traces in some experiments before t = 0 min and always

disappeared after adding the protease solution (i.e. where t > 0 min). Figure S6c shows the ACV trace obtained at t = 1.2 min, which is the first measurement after t = 0 min. Here, the ACV data can be reliably fitted to a single Gaussian peak ($R^2 = 0.943$). The presence of the interference peak at t = 0 min and its subsequent absence at later time causes a decrease in the overall current leading to a large drop in i_p observed at these time points. Consequently, all data analysis and fitting have been performed omitting the measurement at t = 0 min.

Figure 4 shows the results of proteolysis measurements obtained on an MEA where the electrodes were selectively functionalized with peptide H-15. First, the top two rows (CH 1-6) were modified by incubating the electrodes in an aqueous solution containing 1.0 mM mercaptohexanol and 0.2 mM mercaptohexanoic acid for 40 minutes to form a SAM with exposed hydroxyl and carboxyl terminal groups. Next, the SAM modified electrodes were incubated in an aqueous solution containing 0.20 g/l EDC, 0.20 g/l sulfo-NHS and 2.0 mM of the peptide-Fc substrate (H-15) for 2 hours to tether the peptide-Fc to the SAM. The bottom row (CH 7-9) was passivated by forming the SAM and then incubating the electrodes with a solution containing 0.20 g/l EDC, 0.20 g/l sulfo-NHS, but omitting the peptide-Fc substrate. Figures 4a and 4b show the baseline subtracted ACV traces for adjacent SAM/peptide-Fc modified (H-15, CH 4) and a SAM passivated (CH 7) electrodes obtained at various time points. These measurements were performed in a solution containing 25 mM MES buffer (pH = 5.0). Immediately before t = 0, a solution containing 6.0 nM cathepsin B was injected into the electrochemical cell. In Figure 4a, the trace obtained at t = 0.0 min shows a Gaussian-shaped peak with $i_p = 72.5$ nA at -0.05 V vs. MSE. At t = 4.9 min, i_p has decreased to 60.3 nA but the peak position has not changed significantly. This observable decrease in i_p occurs as a result of the cleavage and dissipation of peptide-Fc molecules caused by the proteolysis reaction. As t increases, i_p continues to decrease until it reaches 20.0 nA at t = 40.0 min. The value of i_p further decreases beyond t = 40.0 min.

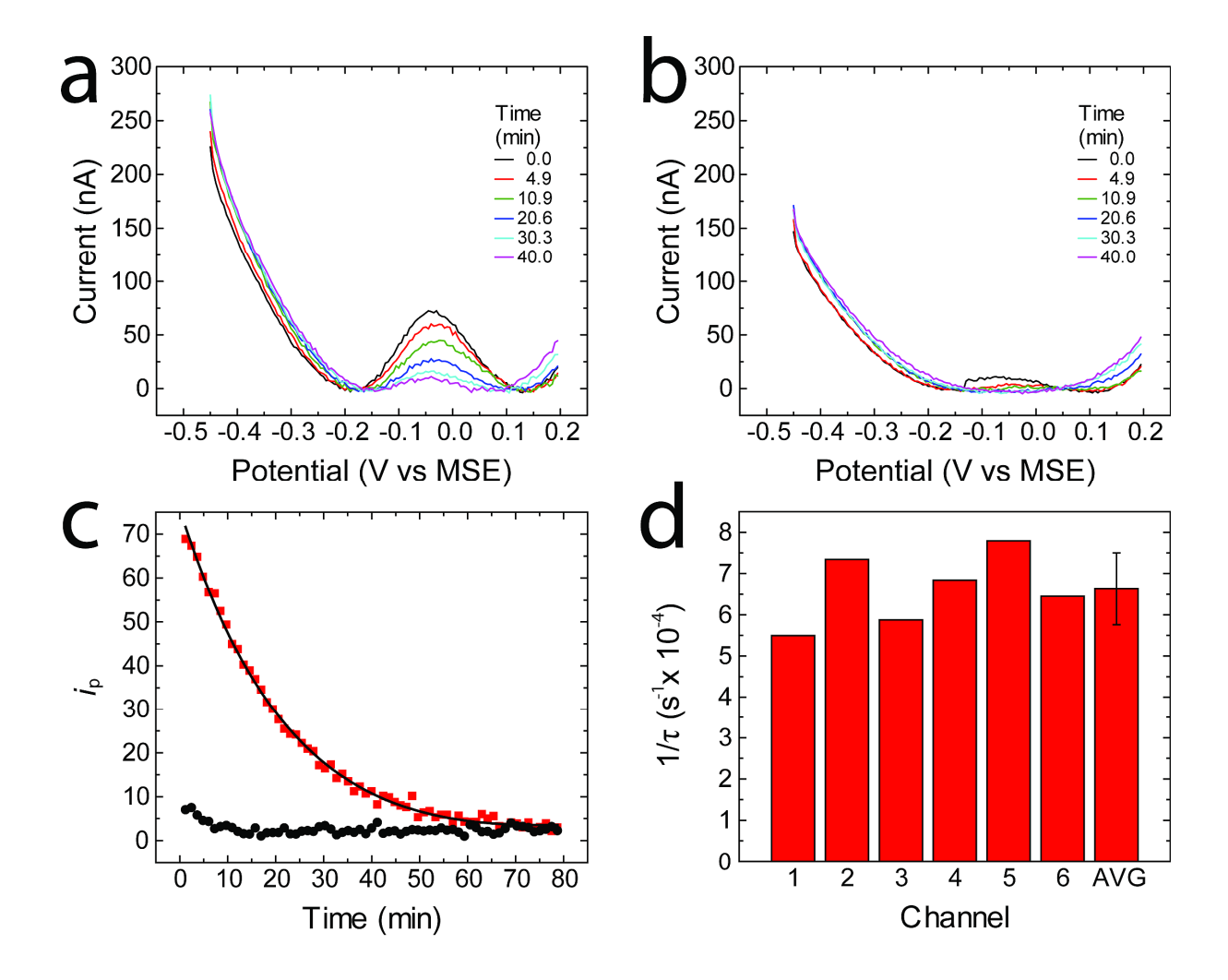


Figure 4: Proteolysis measurements obtained with an Au MEA. Measurements were performed in a solution containing 50 mM MES buffer (pH = 5.0) and 6.0 nM cathepsin B. The protease was injected at t = 0.0 min. (a) ACVs obtained at a microelectrode modified with peptide H-15. (b) ACVs obtained at a control microelectrode, which was passivated with mercaptohexanol/mercaptohexanoic acid and subsequently treated with an aqueous solution containing 0.20 g/l EDC and 0.20 g/l sulfo-NHS. (c) Proteolysis curves showing the relationship between i_p vs. reaction time for the H-15 modified (red squares) and the passivated microelectrodes (black circles) shown in (a) and (b), respectively. The black line represents the exponential fit of the H-15 modified microelectrode using eq. 8. (d) Bar graph showing the fitted values of $1/\tau$ for all of H-15 modified channels (CH 1-6) obtained simultaneously with the data shown in (a), (b) and (c).

Figure 4b shows the control curves obtained on a passivated electrode without peptide-Fc functionalities (CH 7) as described above. These results were obtained simultaneously as the results shown in Figure 4a. Here, at t = 0.0 min, a small (11.9 nA) peak can be observed at -0.06 V vs. MSE. This peak is slightly larger than the background noise and likely due to a small amount of cross-contamination during the modification process. At t = 10.9 min and later, no observable peak can be distinguished from the background signal.

For comparison, Figure S7 shows ACV traces from all nine channels, which were simultaneously obtained during the experiment shown in Figure 4. Each frame shows background subtracted ACV traces obtained before (t = 0.0 min, black trace) and after (t = 79.9 min, red trace) the proteolysis reaction. The traces are plotted on the same scale to highlight the differences between the six SAM/peptide modified electrodes (CH 1-6) and the three SAM modified electrodes (CH 7-9). The six SAM modified electrodes show a Gaussian peak corresponding to the presence of the peptide-Fc substrate bound to the electrode surface. The peak potential (E_p) varies slightly from channel to channel ($E_p = -0.03 \pm 0.01$ V vs. MSE), which is mainly due to variations in background subtraction. The average value of i_p before proteolysis is 93.1 \pm 18.8 nA across all six of the SAM/peptide-Fc modified electrodes. The relatively small variation in i_p is due to the differences in the surface density and conformation of the peptide-Fc tags on the electrode surfaces, which can change with the exposed carboxyl functionalities on the surface and the EDC/NHS coupling efficiency. After proteolysis, there is no obvious peak remaining and the average current at -0.03 V is 1.4 \pm 3.3 nA, which is within the noise of the

measurements. In contrast, the value of i_p measured on the passivated electrodes (CH 7-9) before and after proteolysis was 10.1 ± 9.9 nA and 0.0 ± 6.9 nA, respectively.

Figure 4c shows the proteolysis curves obtained from the data in Figures 4a and 4b. Here the red squares show the results obtained from an electrode, which has been functionalized with the peptide-Fc substrate H-15 (CH 4), and the black line corresponds to the exponential fit of that data. Here, the first data point is not plotted, and is not included in the exponential fit due to the presence of the interference peak as discussed above. The fit shows good agreement with the data ($R^2 = 0.997$) and the fitted value of $1/\tau$ is 6.84 x 10^{-4} s⁻¹. Figure S8 shows the proteolysis curves for all nine channels. Each peptide-Fc functionalized electrode (CH 1-6) shows a clear value of i_p ranging from 65.5 nA to 116.0 nA at the beginning of the proteolysis reaction (t = 1.2 min). Beyond t = 1.2 min, i_p shows a clear exponential decay. The red line shown in the frames corresponding to CH 1-6 are the exponential fits of the data for each channel. For each case, the fit shows good agreement ($R^2 > 0.98$) with the data. In contrast, CH 7-9 does not show any signs of exponential decay and, consequently, no fitting was performed.

Figure 4d is a bar graph representing the measured values of $1/\tau$ for CH 1-6 along with the average and standard deviation across the six channels. The average value of $1/\tau$ is $(6.63 \pm 0.87) \times 10^{-4} \text{ s}^{-1}$. All fitting parameters in eq 8 for each of the six peptide-Fc modified channels are shown in Table S2 along with the calculated value of i_{p0} and the R² of each fit. These results demonstrate that the activity $(1/\tau)$ can be determined reproducibly (RSD = 0.13) and simultaneously on these selectively modified Au MEAs, and that the electrodes on the MEA can be selectively modified and clearly differentiated by ACV with minimal interference and cross-contamination between electrodes.

3.4 Multi-Peptide Measurements:

Single peptide measurements are adequate for quantification of single proteases. However, using different peptide-Fc substrates provide specificity for simultaneous detection of multiple proteases and will allow quantification of the activity profiles for these proteases, which offers enhanced capability for medical diagnosis and health monitoring involving complex samples. Figure 5 shows a series of data obtained with multiple peptide-Fc substrates at once on a single MEA chip. For the experiments depicted here, the top row of electrodes (CH 1 - 3) are modified with peptide H-16, the middle row of electrodes (CH 4 - 6) are modified with peptide H-15, and the bottom row of electrodes (CH 7 - 9) are modified with peptide H-3.

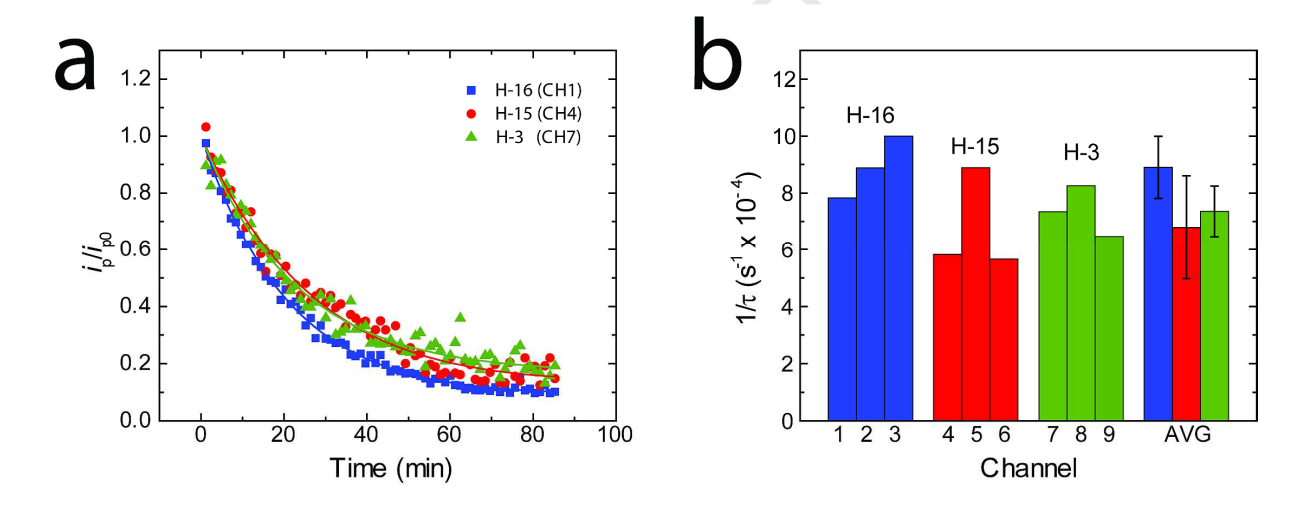


Figure 5: Proteolysis data obtained on an Au MEA chip where CH 1-3 were modified with peptide H-16 (blue), CH 4-6 were modified with peptide H-15 (red), and CH 7-9 were modified with peptide H-3 (green). The experiment was performed in a solution containing 50 mM MES buffer (pH = 5.0) and 6.0 nM cathepsin B. (a) Representative proteolysis curves and fitting lines for electrodes modified with H-16 (CH 1), H-15 (CH 4) and H-3 (CH 7). The data is normalized to the fitted values i_{p0} derived from eq 9. (b) Bar graph showing the fitted values of $1/\tau$ for the channels modified with H-16 (CH 1-3), H-15 (CH 4-6), and H-3 (CH 7-9), respectively, and their average values at the far right with the standard deviation shown as the error bars.

Figure 5a shows examples of proteolysis curves obtained on CH 1 (H-16, blue line), CH 4 (H-15, red line), and CH 7 (H-3, green line). Here, the data is normalized to the value of i_{p0} derived from the fitting data according to eq 9. This normalization accounts for variations in Γ of the peptide-Fc substrate between each of the electrodes, and the values of i_{p0} and values of i_{p0} are listed in Table S3. Each of these proteolysis curves shows a slightly different activity based on the observable rate of decay in i_p . Figure 5b is a bar graph illustrating the differences in the measured values of $1/\tau$ broken down by channels with H-16 (shown in blue), H-15 (shown in red) and H-3 (shown in green), similar to Figure 5a. Here the average values of $1/\tau$ were measured to be $(8.9 \pm 1.1) \times 10^{-4} \text{ s}^{-1}$, $(6.8 \pm 1.8) \times 10^{-4} \text{ s}^{-1}$, and $(7.4 \pm 0.9) \times 10^{-4} \text{ s}^{-1}$ for H-16, H-15 and H-3, respectively. The proteolysis curves of each electrode are shown in Figure S9 and the fitting results for each curve are shown in Table S3. These three peptides show similar values of $1/\tau$ because the majority of the amino acid sequences are similar. As discussed in Figures S10 and S11 in the Supplementary Information, cathepsin B was found to cleave peptide H-15 and H-16 between the Leu-Ala and Pro-Leu, respectively, while peptide H-3 was cleaved in two locations: between Gly-Ala and Phe-Gly residues as revealed by HPLC analyses in our previous study. (Song et al., 2019)

4. **Conclusions:**

We have demonstrated rapid multiplex electrochemical detection of cathepsin B activities through fabrication of an individually addressed 3x3 Au MEA and systematic characterization. The microelectrode arrays were fabricated on 100 mm Si wafers containing 20 MEA chips, each $200 \ \mu m \ x \ 200 \ \mu m$ in size. The chip surface was protected with a $1-\mu m$ thick layer of SiO_2 with only the active electrode surface and the electrical contact areas exposed. Highly consistent

signals among the nine microelectrodes have been obtained in electrochemical cleaning and electrochemical characterization with benchmark redox species. Selective functionalization of the Au microelectrode surface with specific Fc-labeled peptide molecules was achieved. The consistent proteolytic kinetics can be measured by monitoring the decay of the ACV signal of Fc as the peptide molecules are cleaved by cathepsin B. We further demonstrated the simultaneous detection of the proteolysis of cathepsin B on three specific hexapeptides on the same MEA, which can be used for rapid screening of potential peptide candidates. This study has established a sensor platform for future rapid detection of the activity profiles of multiple proteases towards cancer diagnosis.

Acknowledgements

This work was supported by the National Cancer Institute of the National Institute of Health under the award number R01 CA217657, the Johnson Cancer Research Center at Kansas State University, and the Translational Research Institute through Cooperative Agreement NNX16AO69A. The content is solely the responsibility of authors and does not necessarily represent the official views of the National Institutes of Health. The microfabrication work was performed in part in the nano@Stanford labs, which are supported by the National Science Foundation as part of the National Nanotechnology Coordinated Infrastructure under award ECCS-1542152. This material was based upon work in part supported by the National Science Foundation under 1826982 (to DHH and JL) for the purchase of a 400-MHz NMR spectrometer.

Appendix A. Supporting information

Supplementary data associated with this article can be found in the online version at xxx.

References

Anderson, M.J., Crooks, R.M., 2014. Anal. Chem. 86(19), 9962-9969.

Arumugam, P.U., Chen, H., Siddiqui, S., Weinrich, J.A.P., Jejelowo, A., Li, J., Meyyappan, M., 2009. Biosens. Bioelectron. 24(9), 2818-2824.

Bard, A.J., Faulkner, L.R., 2001. Electrochemical Methods: Fundamentals and Applications, 2nd ed. John Wiley & Sons, New York.

Collard, D.M., Fox, M.A., 1991. Langmuir 7(6), 1192-1197.

González-Fernández, E., Avlonitis, N., Murray, A.F., Mount, A.R., Bradley, M., 2016. Biosens. Bioelectron. 84, 82-88.

Gutiérrez, O.A., Chavez, M., Lissi, E., 2004. Analytical Chemistry 76(9), 2664-2668.

Hua, X., Xia, H.-L., Long, Y.-T., 2019. Chem. Sci. 10(24), 6215-6219.

Jacquemier, J., Ginestier, C., Rougemont, J., Bardou, V.J., Charafe-Jauffret, E., Geneix, J., Adelaide, J., Koki, A., Houvenaeghel, G., Hassoun, J., Maraninchi, D., Viens, P., Birnbaum, D., Bertucci, F., 2005. Cancer Res. 65(3), 767-779.

Kang, D., Ricci, F., White, R.J., Plaxco, K.W., 2016. Anal. Chem. 88(21), 10452-10458.

Koblinski, J., Ahram, M., Sloane, B., 2000. Clin. Chim. Acta 291.

Koehne, J.E., Chen, H., Cassell, A.M., Yi, Q., Han, J., Meyyappan, M., Li, J., 2004. Clinic. Chem. 50(10), 1886-1893.

Lee, M., Fridman, R., Mobashery, S., 2004. Chemical Society Reviews 33(7), 401-409.

Leelawat, K., Sakchinabut, S., Narong, S., Wannaprasert, J., 2009. BMC Gastroenterol 9, 30.

Liu, G., Wang, J., Wunschel, D.S., Lin, Y., 2006. Journal of the American Chemical Society 128(38), 12382-12383.

López-Otín, C., Matrisian, L.M., 2007. Nature Reviews Cancer 7, 800.

López-Otín, C., Overall, C.M., 2002. Nature Reviews Molecular Cell Biology 3, 509.

Morris, C.A., Morris, L.D., Kennedy, A.R., Sweeney, H.L., 2005. J Appl Physiol 99(5), 1719-1727.

Nagaraj, N.S., Santhanam, K., 2006. J. Food Biochem. 30(3), 269-291.

Oesch, U., Janata, J., 1983a. Electrochim. Acta 28(9), 1237-1246.

Oesch, U., Janata, J., 1983b. Electrochim. Acta 28(9), 1247-1253.

Ohtsuka, K., Maekawa, I., Waki, M., Takenaka, S., 2009. Anal. Biochem. 385(2), 293-299.

Ong, I.L.H., Yang, K.-L., 2017. Analyst 142(11), 1867-1881.

Podrażka, M., Bączyńska, E., Kundys, M., Jeleń, P.S., Witkowska Nery, E., 2018. Biosensors 8(1), 3.

Puiu, M., Bala, C., 2017. Bioelectrochemistry.

Radke, S.M., Alocilja, E.C., 2005. Biosensors and Bioelectronics 20(8), 1662-1667.

Rakashanda, S., Rana, F., Rafig, S., Masood, A., Amin, S., 2012. Biotech. & Mol. Biol. Rev. 7, 90-101.

Rodríguez-López, J., Alpuche-Avilés, M.A., Bard, A.J., 2008. J. Am. Chem. Soc. 130(50), 16985-16995.

Sanman, L.E., Bogyo, M., 2014. Annu. Rev. Biochem. 83(1), 249-273.

Song, Y., Fan, H., Anderson, M.J., Wright, J.G., Hua, D.H., Koehne, J., Meyyappan, M., Li, J., 2019. Anal. Chem. 91(6), 3971-3979.

Swisher, L.Z., Prior, A.M., Gunaratna, M.J., Shishido, S., Madiyar, F., Nguyen, T.A., Hua, D.H., Li, J., 2015. Nanomedicine: NBM 11(7), 1695-1704.

Swisher, L.Z., Prior, A.M., Shishido, S., Nguyen, T.A., Hua, D.H., Li, J., 2014. Biosens. Bioelectron. 56, 129-136.

Swisher, L.Z., Syed, L.U., Prior, A.M., Madiyar, F.R., Carlson, K.R., Nguyen, T.A., Hua, D.H., Li, J., 2013. J. Phys. Chem. C 117(8), 4268-4277.

Turk, B., 2006. Nat Rev Drug Discov 5(9), 785-799.

Turk, B., Turk, D., Turk, V., 2012. The EMBO Journal 31(7), 1630-1643.

Wang, Z.-y., Zhang, C.-p., Zhang, C.-y., 2020. Chemical Communications.

Wightman, R.M., 1981. Analytical Chemistry 53(9), 1125A-1134A.

Journal Pre-proof

- A 3 x 3 gold microelectrode array chip was fabricated and used as a multiplex sensor
- No significant interference or cross-contamination between electrodes was observed
- Proteolysis kinetics were monitored simultaneously on all nine electrodes
- Activities of the proteolytic reaction by cathepsin B were derived for three peptide substrates

Journal Pre-proof

Declaration of interests
oxtimes The authors declare that they have no known competing financial interests or personal relationships that could have appeared to influence the work reported in this paper.
☐The authors declare the following financial interests/personal relationships which may be considered as potential competing interests: